Total and Radiative Heat Transfer to an Immersed Surface in a Gas-Fluidized Bed

A high-temperature heat transfer probe capable of measuring both the total and radiative heat transfer coefficients between an immersed surface and the bed has been designed, fabricated, and tested. Measurements of these coefficients in beds of 559 and 751 μm sand particles at temperatures up to 1,175 K have been made using this probe. A thermal analysis of the probe is developed in order to ensure a reliable interpretation of the measured quantities. The dependence of the total and radiative heat transfer coefficients on such parameters as bed temperature, fluidizing air velocity, and mean bed particle size are investigated. The various models proposed to describe high-temperature heat transfer are evaluated from this perspective. The models capable of best simulating the heat transfer process with relative ease of computation are identified and evaluated using data generated in the study.

Ajay Mathur, S. C. Saxena
Department of Chemical Engineering
University of Illinois
Chicago, IL 60680

Introduction

The presence of radiation as a mode of heat transfer in high-temperature gas-fluidized beds, along with particle and gas convection, leads to an enhancement of the overall heat transfer rate between the bed and an immersed surface, as compared to that in beds at low and moderate temperatures. This necessitates the development of reliable mechanistic models and simple correlations capable of adequately describing the heat transfer characteristics of the bed at elevated temperatures. High-temperature heat transfer is significantly more difficult to describe since the convective (particle and gas) and radiative modes occur simultaneously and in parallel, and the inclusion of the two processes in a single step becomes difficult due to the nonlinear dependence of radiation on temperature. Due to the industrial interest in fluidized-bed technology, efforts have been made from time to time to measure the total heat transfer coefficient at high temperatures. Various experimental techniques have been used to obtain the value of the total heat transfer coefficient h_w, and the radiative heat transfer coefficient h_{wr}, as a function of bed and surface temperatures, particle size, and fluidizing velocity. These efforts are examined here, and are utilized in developing a high-temperature heat transfer probe for the simultaneous measurement of h_w and h_{wr}.

The results obtained with this probe up to a maximum temperature of 1,175 K for both heat transfer coefficients in fluidized beds of silica sands of average diameters of 559 and 751 μm are reported as a function of fluidizing velocity. The results are examined in the light of the data available in the literature, and also on the basis of the theoretical models. This has enabled the estimation of the relative adequacies of different theoretical models and also helped in resolving some of the existing controversies concerning the parametric dependence of the radiative heat transfer coefficient on different parameters.

Correspondence concerning this paper should be addressed to S. C. Saxena.
Ajay Mathur is with the Tata Energy Research Institute, New Delhi, India.

Heat Transfer Fluxes and Coefficients at High Temperatures

The heat transfer process at high temperatures in gas-fluidized beds consists of particle convection, gas convection, and radiation. The total heat flux from the bed to an immersed surface at a lower temperature is given by:

$$q = (q_{pce} + q_{gce} + q_{re})(1 - f_B) + (q_{gcB} + q_{rB}) f_B \quad (1)$$

$$q_{pc} = q_{pce}(1 - f_B) \quad (2)$$

here,

$$q_{gc} = q_{gce}(1 - f_B) + q_{gcB} f_B \quad (3)$$

and

$$q_r = q_{re}(1 - f_B) + q_{rB} f_B. \quad (4)$$

In general, q_{pce} and q_{gce} are different because the mean boundary layer thickness on the surface is different for the two phases (Ganzha et al., 1982). However, for beds of small particles, groups I and IIA in the particle classification scheme of Saxena and Ganzha (1984), Eq. 1 simplifies to:

$$q = (q_{pce} + q_{re})(1 - f_B) + q_{rB} f_B. \tag{5}$$

For group III particle beds, Eq. 1 simplifies to:

$$q = q_{pce} + q_{gce} + q_{re}. \tag{6}$$

The general form of Eq. 1 must therefore be used for beds of group IIB particles.

The convective and radiative heat transfer coefficients are appropriately defined as:

$$h_{wc} = (q_{pc} + q_{gc})/(T_b - T_t) \tag{7}$$

and

$$h_{wr} = q_r/(T_l - T_t). \tag{8}$$

The total heat transfer coefficient, h_w, is

$$h_w = h_{wc} + h_{wr}. \tag{9}$$

For group III particle beds, Eq. 8 may be written as:

$$h_{wr} = q_r/(T_b - T_t). \tag{10}$$

and h_w on the basis of Eqs. 7, 8, and 4 as

$$h_w = q/(T_b - T_t). \tag{11}$$

In practice, however, Eq. 11 is used for beds of particles of all sizes as an approximation since T_l is difficult to measure. In the present study, Eqs. 10 and 11 are used to determine h_{wr} and h_w, respectively.

Experimental Procedure

Measurement of h_w *and* h_{wr}

The total and radiative heat transfer coefficients between a fluidized bed and an immersed surface at high temperatures have been measured by a limited number of workers; the results are listed in a historical sequence in Table 1. The table also identifies the experimental techniques used by each investigator as well as the ranges of average particle sizes and temperatures. The measurement techniques for h_w and h_{wr} may be divided into three different categories in both cases. For h_w these are:

I. Methods employing the change in temperature with time of a heated metallic probe immersed in the bed

II. Methods using a fluxmeter

III. Methods exploiting a water-cooled probe

The three categories for h_{wr} measurement are:

1. Methods employing a quartz or silica window to block the convective flux and allow only the radiative flux to reach a fluxmeter

2. Methods involving the measurement of heat transfer by two probes of high and low emissivities

Table 1. Investigations of High-Temperature Heat Transfer in Gas-Fluidized Beds

Investigators	Measurement Method Category h_w	Measurement Method Category h_{wr}	$\bar{d}_p$ μm	T_b K
Jolley (1949)	I	—	800	1,048–1,253
Il'chenko et al. (1968)	II	1	570–1,750	700–1,700
Szekely & Fisher (1969)	—	3	200–300	<600
Wright et al. (1970)	III	—	1,800–2,900	1,073–1,173
Baskakov et al. (1973)	I, II	—	350–1,250	1,123
Yoshida et al. (1974)	III	2	180	823–1,273
Thring (1977)	III	—	582, 928	923–1,273
Basu (1978)	II	1	325–500	973–1,273
Panov et al. (1979)	I	2	500–6,000	800–1,200
Vadivel & Vedamurthy (1980)	II	1	4,000–6,000	1,023
Flamant (1982)	—	3	250	600–1,400
Botterill et al. (1984)	I, II	2	370–3,000	573–1,273
George & Welty (1984)	II	—	2,140;3,230	810–1,005
Ozkaynak et al. (1984)	II	1	1,030	<760
Zhang et al. (1984)	II	—	1,340–1,580	1,073–1,273
Alavizadeh et al. (1985)	II	1	520–3,230	812–1,050
Goshayeshi et al. (1985)	II	—	2,140, 3,230	810–1,005
Tuzla et al. (1985)	II	—	465–1,400	773
Zhang & Xie (1985)	II	1	1,000;4,000	1,073–1,313

3. Methods involving passing of the radiative flux only in the bed and measuring the resulting temperature change

For well-known reasons, category I methods for h_w measurement have been found to yield greater h_w values than the methods of categories II and III (Baskakov et al., 1973; Botterill et al., 1984). Category III probes have been found to yield unreliable values due to large uncertainties in temperature measurement of the coolant outlet stream (White et al., 1986). Category II methods, which employ a fluxmeter, appear to be most attractive for the measurement of h_w. Obviously simultaneous measurement of h_w and h_{wr} is most desirable and this eliminates category 3 methods. Category 2 methods are likely to yield erroneous results owing to the change in surface emissive properties with time due to abrasion of the probe surface by particles. The use of a quartz glass window to isolate the convective flux, characteristic of category 1 methods, is, therefore, adopted here. The general drawback of this technique is that the finite conductivity of quartz glass causes some convective flux to be conducted to the fluxmeter. However, the convective flux can be either reduced by experimental arrangement, or accurately estimated by a detailed calculation.

Design of high-temperature heat transfer probe

In the perspective of the above discussion, a probe for the measurement of the total heat transfer and its radiative component at high temperatures has been designed and developed. The probe, shown in Figure 1, has a nominal diameter of 66.3 mm and comprises a water inlet section *A*, fluxmeters *B* and *C*, and water outlet section *D*. The middle section of the probe accommodates the two fluxmeters, each housed in a 304 stainless steel 50.8 mm dia. tube. These tubes are transversely inserted into the

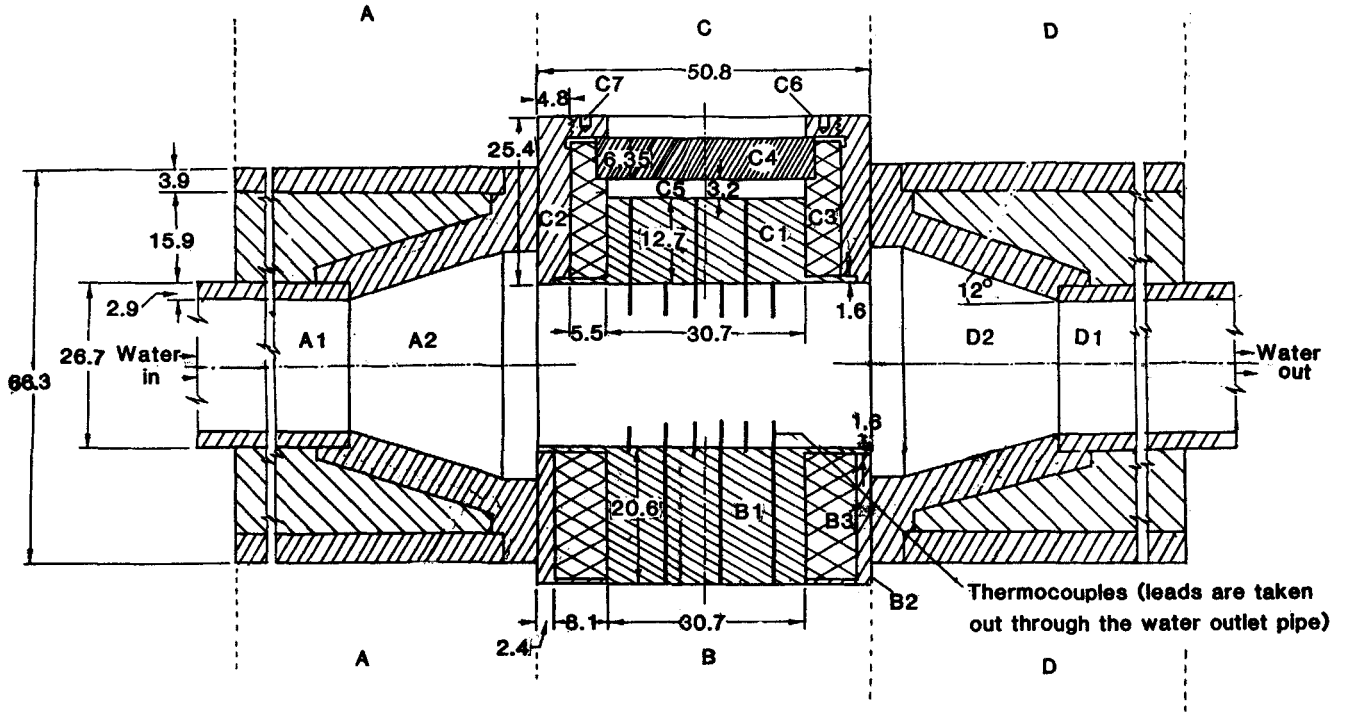

Figure 1. High-temperature heat transfer probe.

main probe, a 66.3 mm OD, 3.9 mm thick, 304 stainless steel pipe. The lengths of the tubes housing fluxmeters *B* and *C* are 20.6 and 25.4 mm, respectively. The thickness of these tubes are 2.4 and 4.8 mm, respectively.

The water inlet section, *A*, consists of the water intake pipe, *A1*, of 304 stainless steel, having a 26.7 mm OD and a thickness of 2.9 mm, which is insulated from the probe pipe by a layer of Fiberfrax T-30R insulation 15.9 mm thick. The purpose of the diverging section, *A2*, is primarily to provide mechanical support to the water intake pipe, *A1*, as well as to smooth out the water flow past the interior faces of the fluxmeters. The space between the diverger section and the probe pipe is also filled with insulating Fiberfrax Lo-Con felt. The water outlet section, *D*, is similar to water inlet section *A* both in design and purpose. The water flows out of the reducer section, *D2*, and the water outlet pipe, *D1*.

Fluxmeter *B*, designed to measure the total heat flux and the total heat transfer coefficient, is a 30.7 mm dia. 420 stainless steel plug, *B1*, inserted into the main housing pipe, *B2*, and insulated from it by a 8.1 mm thick annular ring of Zircar thermal insulation, *B3*. It is recognized that some thermal leakage will take place from the interior face of the fluxmeter from *B1* to *B2*, and this has been minimized by reducing the thickness of the extending shoulder of *B1*. The thermal conductivity of the plug material, k_p, as well as its thickness, x_b, are precisely known, and the temperature difference across it, $(T_{Bo} - T_{Bi})$, is measured by a set of six thermocouples, three on each of the two faces. The thermal conductivity of stainless steel 420 at various temperatures ranging from 435 to 1,630 K has been taken from the tabulation of Touloukian et al. (1970).

The thermal fluxmeter, *C*, designed to isolate and measure the radiation component of total heat flux and the radiative heat transfer coefficient, is also a plug of 420 stainless steel, 30.7 mm in dia. and 12.7 mm thick. Its design is similar to that of *B* in many respects but is more complicated. A 6.35 mm thick polished quartz glass window, *C4*, is incorporated to isolate the thermal radiation from the total incident thermal flux, and only the former is transmitted to plug *C1*. The thermal conductivity of the quartz glass is 1.38 W/mK. Plug *C1* is welded to the main housing pipe, *C2*, with a Zircar insulation lining, *C3*, in between. The thickness of this thermal insulation lining is 5.5 mm. The quartz window, *C4*, is held tightly on a shoulder of Zircar insulation via a threaded ring, *C6*, mating with threads in pipe housing *C2*. The ring rotation is accomplished through two pinholes, *C7*. The air gap, *C5*, between the quartz window, *C4*, and the exterior face of plug *C1* is 3.2 mm thick. The heat conduction or natural convection occuring in this air film augmenting the heat transfer process is corrected by a theoretical calculation. Not all the thermal radiation incident on the quartz window is transmitted to plug *C1* for measurement: a part is scattered and absorbed. These losses are accounted through knowledge of the transmissivity of the quartz glass. The transmissivity chart for quartz glass has been supplied by the manufacturer. The temperatures of the two faces of plug *C1* are established by six thermocouples, as in the case of *B1*.

The thermocouples used in the heat transfer probe are chromel-alumel (K-type), and are encased in grounded Inconel sheaths filled with magnesium oxide as an electrical insulator. The thermocouple leads are brought out through the water outlet pipe and are connected to a Leeds and Northrup 934 Numatron with a 16-point switch for digital display.

Thermal analysis of the high-temperature heat transfer probe

The water flowing through the probe removes the heat added through the two fluxmeters, and enables the setting up of thermal equilibrium in both meters. The fluxes incident on the probe

are given by:

$$q = k_p(T_{Bo} - T_{Bi})/x_B \tag{12}$$

and

$$q_C = k_p(T_{Co} - T_{Ci})/x_C \tag{13}$$

respectively. T_{Bo} and T_{Co}, and T_{Bi} and T_{Ci} are the temperatures of the outer and inner surfaces of fluxmeters B and C, respectively. x_B and x_C are the thicknesses of the two fluxmeters. The total heat transfer coefficient and its radiative component are calculated from the following relations:

$$h_w = q/(T_b - T_{Bo}) \tag{14}$$

and

$$h_{wr} = q_r/(T_b - T_{Bo}), \tag{15}$$

q_r is the radiative heat flux incident on fluxmeter C, and is obtained from q_C after applying a correction for the convective flux leakage.

The flux measured by fluxmeter C, q_C, comprises the fraction of the radiative flux that is transmitted through the quartz glass window, and the leaked convective flux, q_1, which has been conducted through the quartz glass and the air gap. Thus:

$$q_C = t_q q_r + q_1. \tag{16}$$

Here, t_q is the transmissivity of the quartz glass, q_C, q_r, and q_1 are the fluxmeter measured, radiative, and conductive fluxes, respectively. It is assumed that the air gap $C5$ is transparent to thermal radiation. The value of t_q for the quartz glass employed in the probe construction is from the transmissivity chart provided by the manufacturers, and q_C is calculated using Eq. 13. Thus, in order to obtain q_r it is necessary to obtain q_1 in Eq. 16. This is accomplished according to the procedure detailed in the following.

Figure 2 shows a schematic representation of the heat propagation process and the temperature distribution in fluxmeter C. Radiative flux q_r and convective flux q_{1o} emanate from the bed at temperature T_b, traverse the emulsion phase thermal boundary layer, and are incident on the outer face of the quartz glass, which is at a temperature T_{qo}. The two fluxes simultaneously propagate through the quartz glass, where due to simultaneous scattering and absorption, some of the radiative flux is converted to conductive flux. Thus, $t_q q_r$ is the radiative flux that leaves the inner face of the quartz window, which is at a temperature T_{qi}, and finally reaches the fluxmeter. The conductive flux through the glass is enhanced by the partial conversion of the radiative flux, and the conductive flux leaving the glass and reaching the fluxmeter is given by:

$$q_1 = q_{1o} + (1 - t_q)q_r. \tag{17}$$

Combining Eqs. 16 and 17 to eliminate q_r gives:

$$q_1 = q_{1o} + q_C(1 - t_q)/t_q. \tag{18}$$

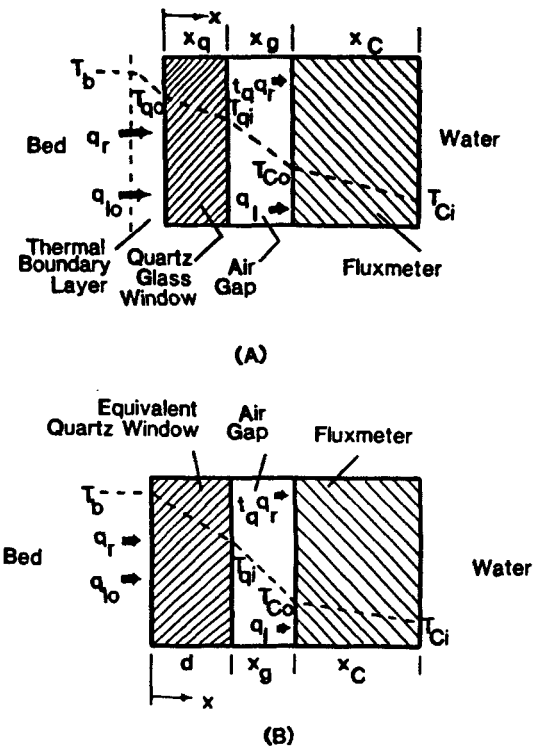

Figure 2. Heat propagation.
A. Radiative fluxmeter; B. An equivalent of (A)
- - - Temperature distribution

Flux q_1 is conducted across the air gap to the fluxmeter, and therefore:

$$q_1 = (k_g/x_g)(T_{qi} - T_{Co}) \tag{19}$$

where T_{qi} and T_{co} are the temperatures of the inner face of the quartz window and of the outer face of the fluxmeter, respectively. The evaluation of q_1 from Eq. 19 requires knowledge of T_{qi}. In order to calculate T_{qi}, the temperature distribution in the quartz glass needs to be established. The temperature of the outer face of the glass can be calculated from:

$$q_{1o} = h_{wc}(T_b - T_{qo}), \tag{20}$$

where h_{wc} is the convective heat transfer coefficient between the bed and the probe. To relate T_{qo} and T_{qi}, the simultaneous conduction-radiation process through glass needs to be formulated so that the temperature distribution in the quartz glass, $T_q(x)$, can be evaluated. The approach of Kellett (1952) is followed here, according to which, for a gray glass,

$$k_q \frac{d^2T_q}{dx^2} - 2\alpha\sigma T_q^4 - \alpha^2 k_q T_q - \alpha^2 q_C x + \alpha C_1 = 0. \tag{21}$$

α is the absorptivity of glass, k_q is its thermal conductivity, and C_1 is an undetermined constant. Here, x is the axial distance in the glass, measured from its outer face as shown in Figure 3A. $T_q(x)$ can be obtained from Eq. 21 when solved with the following boundary conditions:

$$T_q = T_{qo} \quad \text{at} \quad x = 0 \tag{22}$$

$$T_q = T_{qi} \quad \text{at} \quad x = x_q \tag{23}$$

and

$$-k_q \frac{dT_q}{dx} = q_1 \quad \text{at} \quad x = x_q. \tag{24}$$

Thus, $T_q(x)$ can be obtained in terms of q_1, T_{qo}, and T_{qi}. Therefore, Eq. 20 (with Eq. 18), Eq. 19, and the solution for $T_q(x)$, will form a set of three equations whose solutions will yield the values of q_1, T_{qo}, and T_{qi}. The substitution of q_1 in Eq. 16 will yield the value of q_r.

In order to make this approach more mathematically tractable, the above problem is converted into an equivalent problem by lumping together the heat transfer resistances of the emulsion phase boundary layer and the quartz glass. The overall heat transfer process across these two resistances is equivalent to the simultaneous conduction-radiation process occurring across a quartz glass of equivalent thickness d and absorptivity α, where

$$d = x_q + (k_q/h_{wc}) \tag{25}$$

and

$$\alpha = \exp(-t_q/d). \tag{26}$$

h_{wc} has been calculated from the correlation due to Grewal and Saxena (1980). A schematic representation of this heat transfer process is shown in Figure 2B. The temperature variation across the equivalent quartz slab is again described by Eq. 21, but the boundary conditions are:

$$T_q = T_b \quad \text{at} \quad x = 0 \tag{27}$$

$$T_q = T_{qi} \quad \text{at} \quad x = d \tag{28}$$

and

$$-k_q \frac{dT_q}{dx} = q_1 \quad \text{at} \quad x = d. \tag{29}$$

An analytical solution of Eq. 21 is not possible due to the presence of the T_q^4 term, and therefore the following approximation is introduced whose implications and validity are discussed later:

$$T_q^4 = 4T_q\overline{T}_q^3 - 3\overline{T}_q^4. \tag{30}$$

$\overline{T}_q$ is the average temperature in the glass. With Eq. 30, Eq. 21 transforms to:

$$k_q \frac{d^2T_q}{dx^2} - (\alpha^2 k_q + 8\alpha\sigma\overline{T}_q^3)T_q = \alpha^2 q_C x - \alpha C_1 - 6\alpha\sigma\overline{T}_q^4. \tag{31}$$

The solution of Eq. 31 is

$$T_q = C_2 e^{bx} + C_3 e^{-bx} - [(\alpha^2 q_C x - \alpha C_1 - 6\alpha\sigma\overline{T}_q^4)/b^2 k_q]. \tag{32}$$

Here,

$$b^2 = \alpha^2 + (8\alpha\sigma\overline{T}_q^3/k_q), \tag{33}$$

and C_2 and C_3 are constants of integration. The solution of Eq. 32 is valid only in the region of x where Eq. 30 holds. The value of T_q^4 predicted by Eq. 30 is within ±10% of the actual T_q^4 values as long as the following condition is satisfied:

$$0.89\overline{T}_q < T_q < 1.18\overline{T}_q. \tag{34}$$

From Eqs. 27–29, the values of C_1, C_2, and C_3 in Eq. 32 are found to be:

$$C_1 = [T_b - C_4 - (6\alpha\sigma T_q^4/b^2 k_q) - C_2(1 + e^{2bd})]/(\alpha^2/b^2 k_q) \tag{35}$$

$$C_2 = [T_b - T_{qi} - C_4(1 - e^{-bd}) - (\alpha^2 q_C d/b^2 k_q)]/(1 + e^{2bd} - 2e^{bd}) \tag{36}$$

and

$$C_3 = C_2 e^{2bd} + C_4. \tag{37}$$

Here,

$$C_4 = (q_1/bk_q e^{-bd}) - (\alpha^2 q_C/b^3 k_q e^{-bd}). \tag{38}$$

q_1 may now be calculated adopting the following iterative procedure:

1. q_1 is assumed to be a fraction of q_C (0.5 at high bed temperatures; 0.9 at low temperatures).
2. The assumed value of q_1 is substituted in Eq. 38, and the constants C_1, C_2, and C_3 are calculated.
3. T_{qi} is determined from Eq. 32 by setting x equal to d and substituting the values of C_1, C_2, C_3.
4. q_1 is calculated from Eq. 19.
5. The calculated value of q_1 from step 4 is compared with the assumed value. If $q_{1calc} - q_{1ass}/q_{1calc} > 0.01$, then q_{1calc} is taken to be the new value of q_{1ass}, and steps 2–5 are repeated. Once the inequality is no longer satisfied, the iterative process is stopped. q_{1calc} is then substituted as q_1 in Eq. 16, and q_r determined.

Fluidized-bed facility

The probe is mounted in a 0.152 m ID fluidized bed, details of which are described by Saxena and Mathur (1985). The top end of the column is disconnected from the off-gas cleanup system to enable direct viewing of the combustion characteristics and quality of fluidization in the bed. The fluidization column is made of a 25.4 cm dia. column of schedule 40, 304 stainless steel pipe, and is built in four flanged sections, each 57 cm long and bolted together with 3.8 cm longer spacer rings. These sections are placed over a specially designed distributor plate below which is a 30.5 cm long calming section. The high-temperature heat transfer probe is mounted horizontally in the bed through the first spacer ring above the distributor. The top view of the probe as seen in the bed is shown in Figure 3. Four external band heaters are wrapped around the column in the test bed section over a length of about 31 cm along the wall above the distributor plate. These heaters are used to make up for the heat losses from the column wall and thus maintain the bed at the desired constant temperature. The column wall is thermally insulated by three 2.5 cm thick layers of insulation, two on the inside surface, and one on the outside surface. The distributor plate has 19 bub-

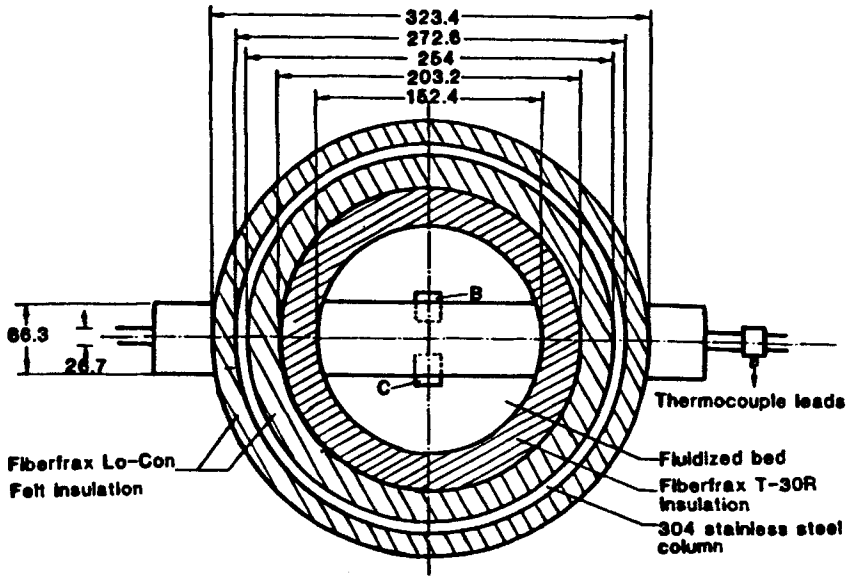

Figure 3. Cross-sectional view of 0.152 m ID bed showing location of high-temperature heat transfer probe.

ble caps located at the vertices of equilateral triangles of 2.9 cm to a side. Each bubble cap is a 2.6 cm dia. stainless steel cylinder with a conical head and a 0.6 cm dia. axial blind hole. The gas exits from the top through eight equally spaced 0.1 cm dia. holes drilled radially, 7.9 cm above the distributor plate.

A metered amount of propane is introduced into the calming section through two nozzles oriented with their discharge ends at an angle of 120°, and located 23 cm below the distributor plate. The nozzles are fabricated from 1.9 cm dia. steel plugs having a tapered conical hole. The propane gas mixes with the fluidizing air in the calming section, and is ignited by an electric igniter in the bed section just above the gas distributor. Six thermocouples are installed to monitor and measure the temperatures in different sections of the fluidization column. Six pressure probes are also provided along the column wall.

Experimental runs

The major operations of a typical experimental run consist of the following steps. The controllers on the preheater and band heaters are adjusted to proper settings for bed temperatures in the range 300–525 K. For higher temperatures, suitably prepared mixtures of propane and preheated air are ignited in the empty bed. A stoichiometric mixture of propane-air is found to bring the bed to a temperature of about 1,250 K. The theoretical flame temperature of such a mixture is 2,600 K. Increasing the propane concentration in the mixture above the stoichiometric value is found to cause the flame front to move up in the column and away from the igniter. Finally, the flame front moves out of the column and the flame extinguishes. Consequently, in our experiments the propane-to-air ratio was never greater than $1/25$. Increasing the proportion of air in the mixture above the stoichiometric value produces bed temperatures lower than 1,250 K. A mixture containing 100% excess air produces a bed temperature of about 700 K. It is also found that when the excess air is more than 100% (propane-to-air ratio less than $1/50$), the flame extinguishes. The steady state is assumed to have been reached when the temperature change as indicated by the thermocouple located 15 cm above the distributor plate is less than ± 1 K over a period of 5 min. The temperature registered by the thermocouple located 10 cm above the distributor plate never differs by more than 2 K from the temperature indicated by the thermocouple at the 15 cm level. The latter is always smaller than the former. At the steady state, in addition to these temperatures the distributor pressure drop, the total pressure drop, and the pressure drop across two sections of the bed are recorded. For the same bed temperature, the air flow rate is reduced, maintaining the same ratio of propane to air in the mixture to obtain data at a different flow rate. The variations in the bed temperature are within ±18 K for the whole range of gas flow measurements.

Results and Discussion

Heat transfer experiments have been conducted in beds of 559 and 751 μm sand particles. The size distribution of these two bed particles is given in Table 2; the temperatures as well as the bed properties at minimum fluidization are listed in Table 3. At each bed temperature, the temperatures T_{Bo}, T_{Bi}, T_{Co}, and T_{Ci} are measured for various values of the fluidizing velocity. The calculated values of h_w and h_{wr} for the two beds are shown in Figures 4 to 7, in each case for various temperatures and fluidizing velocities. h_w is found to increase with increases in T_b. This increase can be attributed to two sources: to the increase in gas

Table 2. Sieve Analysis of Sand Particles

Sieve Opening μm	Mass Fraction of Particles Retained on Sieve	
1,000	0.101	0.001
850	0.296	0.265
600	0.560	0.495
500	0.034	0.192
425	0.004	0.460
355	—	0.001
$\bar{d}_p$	751	559

Table 3. Properties of Particles and Beds at Minimum Fluidization at Various Temperatures

$\bar{d}_p$ μm	ρ_s kg/m³	C_{ps} J/kg · K	T_b K	U_{mf} m/s	ϵ_{mf}
559	2,670	800	385	0.21	0.45
			495	0.18	0.46
			675	0.16	0.46
			820	0.14	0.45
			985	0.14	0.46
751	2,670	800	395	0.40	0.41
			510	0.45	0.47
			675	0.47	0.52
			785	0.53	0.56
			915	0.56	0.57
			1,175	0.72	0.58

thermal conductivity at higher temperatures, which leads to increases in q_{pce}, q_{gce}, and q_{gcB}, and to higher radiative fluxes, q_{re} and q_{rB}, because of the larger value of $(T_l^4 - T_t^4)$.

The variation of h_w with $\bar{d}_p$ follows a more complex trend. At comparatively low bed temperatures (773–823 K), Panov et al. (1979), Botterill et al. (1984), George and Welty (1984), and Tuzla et al. (1985) found h_w to decrease as $\bar{d}_p$ increased from about 465 to about 6,000 μm. The decrease was quite rapid for beds with average particle sizes less than about 1,500 μm, but thereafter the decrease became quite gradual for larger values of $\bar{d}_p$. For higher bed temperatures (>1,000 K) and for values of $\bar{d}_p$ up to about 1,150 μm, an initial decrease in h_w with increase in $\bar{d}_p$ has been observed (Thring, 1977; Panov et al., 1979; Botterill et al., 1984). For $\bar{d}_p$ greater than 1,150 μm, h_w increased (or remained constant) with increase in $\bar{d}_p$ (Wright et al., 1970; Vadivel and Vedamurthy, 1980; George and Welty, 1984; Zhang et al., 1984). Consequently, the difference between h_w values at low and high temperatures is found to increase with increase in particle size. Basu (1978) attributed this trend to the smaller change in T_l in beds of small particles due to a change in T_b, as compared to that in large particle beds. This causes radiative flux to be comparatively small in small particle beds, as compared to that in large particle beds at the same bulk bed temperature. Consequently, the difference in h_w values at low and high temperatures goes on increasing as $\bar{d}_p$ increases. From the data generated in the present study, a comparison of the values of h_{wmax} for the two particles at 675 K shows that h_{wmax} for the bed of 559 μm sand is greater than that for the bed of 751 μm sand, as expected.

The dependence of h_w on U is not quite unambiguous. Wright et al. (1970), Basu (1978), Vadivel and Vedamurthy (1980), Alavizadeh et al. (1985), and Tuzla et al. (1985) have found $h_w$to initially increase with increase in U, and then become constant. The average bed particle size of these investigators ranged

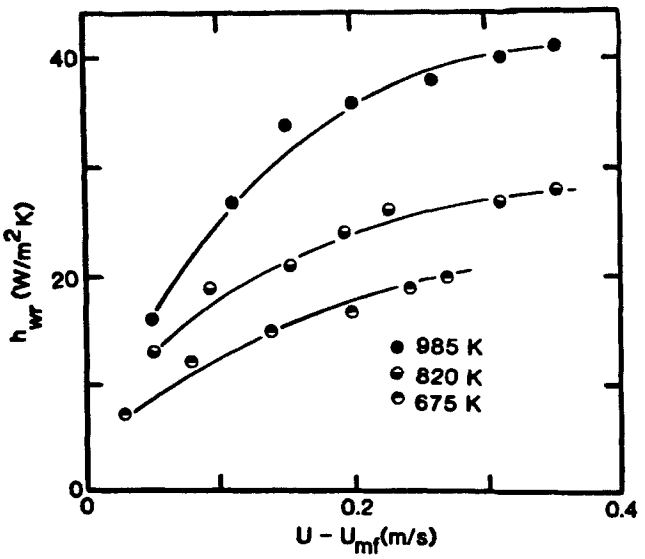

Figure 5. Variation of h_{wr} with $U - U_{mf}$ at three bed temperatures.
559 μm sand particle bed

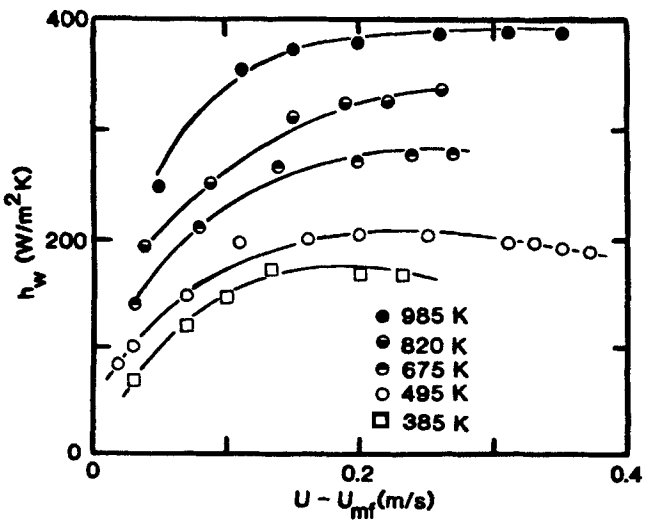

Figure 4. Variation of h_w with $U - U_{mf}$ at five bed temperatures.
559 μm sand particle bed

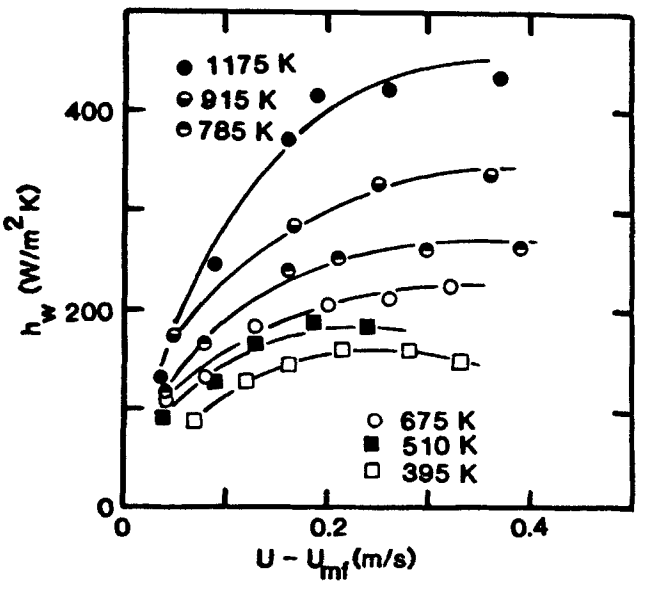

Figure 6. Variation of h_w with $U - U_{mf}$ at five bed temperatures.
751 μm sand particle bed

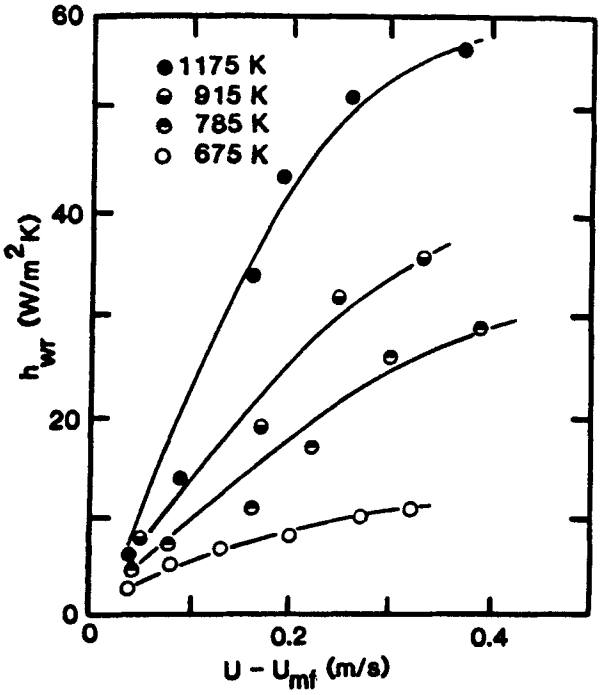

Figure 7. Variation of h_{wr} with $U - U_{mf}$ at four bed temperatures.
751 μm sand particle bed

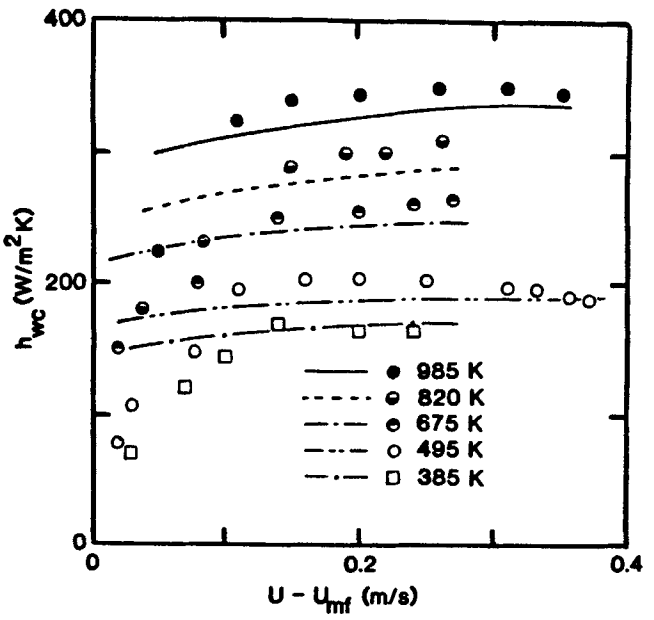

Figure 8. Comparison of experimental h_{wc} values with predictions from correlation of Grewal and Saxena (1980).
559 μm sand particle bed

from 400 to 5,000 μm, and bed temperature from 773 to 1,223 K. Botterill et al. (1984) found a similar trend for a bed of 1,150 μm alumina at 1,153 K, but found h_w to continuously increase with increase in U for a bed of alumina at 773 K up to a U/U_{mf} value of about 10. On the other hand, Zhang et al. (1984) found h_w to decrease as U was increased in the range of $3.5 < U/U_{mf} < 4.5$ for a bed of 1,340 μm particles. It is not possible to explain this discrepancy at this time on the basis of the available details.

The effect of U on q_r is also the subject of some controversy. Il'chenko et al. (1968), Baskakov et al. (1973), Basu (1978), and Ozkaynak et al. (1984) did not observe any variation in h_{wr} as U was changed. However, Szekely and Fisher (1969), Flamant (1982), Botterill et al. (1984), Alavizadeh et al. (1985), and Zhang and Xie (1985) found h_{wr} (or q_r) to increase with increase in U.

The variation of h_w and h_{wr} with U clearly shows the effect of increased bed voidage on radiation. h_{wr} initially increases rapidly as U is increased beyond U_{mf}, but then the increase becomes much more gradual as U increases further. This indicates that once the bed is well fluidized, further increase in U has only marginal effect on h_{wr}. It is also interesting to note that the presence or absence of radiation is also clearly indicated by the trend of the h_w–U curves. The data at the lower temperatures ($T_b < 675$ K), where radiation has been found to be negligible, show that h_w initially increases with increase in U, becomes approximately constant, and then decreases slowly as U is increased further. By contrast, at the higher bed temperatures (>675 K), h_w is never observed to decrease with increase in U. This is due to the contribution of h_{wr}, which increases continuously with increase in U. This variation of h_w with U is examined in the following from the perspective of the correlation of the experimentally calculated h_{wc} ($= h_w - h_{wr}$) values with the predictions based on the correlation of Grewal and Saxena (1980) over the entire ranges of U and T_b.

Figures 8 and 9 show the variation of the experimentally calculated h_{wc} values with U for the two particles at different temperatures. The predicted values of h_{wc} obtained from the correlation of Grewal and Saxena are also shown. The correlation overpredicts the experimental data for the smallest value of $(U - U_{mf})$, but for all the data obtained for $U/U_{mf} > 1.2$ the agreement is within 25%. The stated accuracy for the correla-

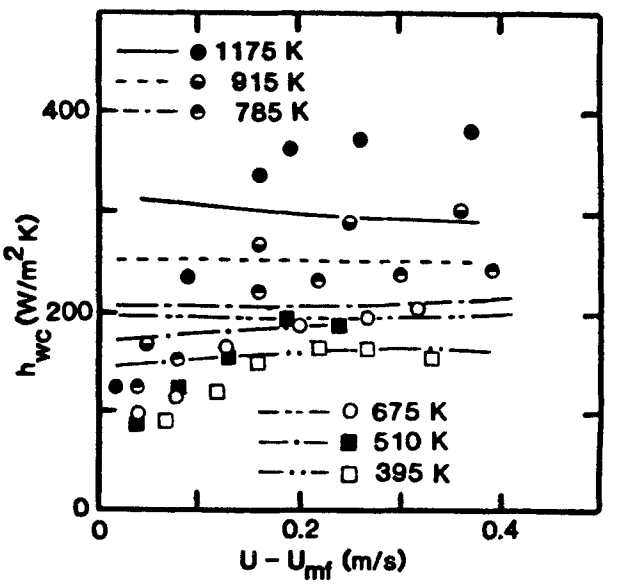

Figure 9. Comparison of experimental h_{wc} values with predictions from correlation of Grewal and Saxena (1980).
751 μm sand particle bed

tion is also ±25%. It is therefore, concluded that the correlation of Grewal and Saxena is capable of predicting the convective component of the heat transfer coefficient with adequate precision even at high temperatures.

In order to evaluate the measurements obtained from the fluxmeter, the present results are compared with those of other investigators obtained for comparable operating conditions. Thring (1977) measured the total heat transfer to beds of 582 and 928 μm particles at 1,100 K. The measured h_w values ranged from 550 to 635 W/m^2 · K for the 582 μm bed, and from 470 to 625 W/m^2 · K for the 928 μm bed. In the present study, h_{wmax} is found to be about 400 W/m^2 · K for the 559 μm bed at 985 K. The trend in the increase of h_{wmax} with T_b indicates that h_{wmax} would be about 470 W/m^2 · K at 1,100 K for this bed. This is lower than the range of values obtained by Thring. This difference is probably due to the difference in the placement of the heat transfer probe in the two investigations. The probe used by Thring was lowered vertically into the bed, whereas in the present study, the probe has been placed horizontally in the bed. The presence of Thring's vertical probe in the 0.152 m ID bed probably used turbulent mixing in the narrow annular bed, leading to higher values of h_w (White et al., 1986). Tuzla et al. (1985) found h_{wmax} to be about 400 W/m^2 · K for a bed of 465 μm sand at 773 K. By comparison, the h_{wmax} value for the 559 μm particle bed is interpolated about 300 W/m^2 · K at 773 K. The lower value is expected as it corresponds to a larger average particle size. The measurements of Alavizadeh et al. (1985) indicate a h_{wmax} value of 349 W/m^2 · K for a 520 μm grain bed at 812 K. A corresponding value of 355 W/m^2 · K is found in the present study for the 559 μm bed at 820 K. However, the value of h_{wr} obtained by Alavizadeh et al. for this condition is 18 W/m^2 · K; the comparable value obtained in this investigation is 28 W/m^2 · K. These comparisions, which are by no means exact, show that the present probe measurements are in the range of reported literature data.

Evaluation of High-Temperature Heat Transfer Models

Various models have been developed to describe the high-temperature heat transfer process in gas-fluidized beds. The models can be classified into three categories depending on how the emulsion phase is modeled. The first category models treat the emulsion phase as discrete particles, the second as a continuum with averaged properties, and the third as a stack of plane-parallel plates. Szekely and Fisher (1969) developed a first category model in which heat transfer is assumed to occur between the surface and the first row of particles. The model predicts radiation to be insignificant at temperatures less than 1,273 K.

The second category models are due to Yoshida et al. (1974), Chen and Chen (1981), and Glicksman and Decker (1985). The models of Yoshida et al. and Glicksman and Decker are similar inasmuch as both consider the emulsion phase heat transfer to be described by the packet model (Mickley and Fairbanks, 1955). The additional heat transfer in the packet due to radiation is accounted for in both models by the use of an enhanced effective bed thermal conductivity that accounts for particle convective and radiative components of heat transfer. The model of Yoshida et al. calculates the radiative flux in the bubble phase by modeling it as radiative transfer between a hemispherical surface and its equatorial plane, both at constant although different temperatures. The model of Glicksman and Decker introduces an additional thermal resistance in the form of a gas film between the immersed surface and the packet (Gelperin and Einshtein, 1971). Chen and Chen modeled the heat transfer process by a nonlinear differential formulation of the simultaneous radiative-conductive flux in the emulsion packet. The radiative flux in the emulsion is described by the two-flux model, which assumes a forward flux and a backward flux to traverse the emulsion undergoing absorption and scattering. The general limitation of the second category models is that they require knowledge of averaged bed properties such as effective bed thermal conductivity, packet residence time, and bubble fraction. In addition, the more rigorous model of Chen and Chen requires the bed absorption and scattering cross sections, which are difficult to evaluate.

The third category models evaluate heat transfer between arbitrarily defined bed regions, each separated from the other by a plane-parallel plate. Thus, Vedamurthy and Sastri (1974) assume radiation to occur only between adjacent plates, along with conduction through the emulsion phase between the plates. The emulsion phase is assumed transparent to radiation. Bhattacharya and Harrison (1977) modified the model of Vedamurthy and Sastri by assuming the emulsion to participate in the radiative transfer, and each plate to radiatively interact with 25 plates on either side. Thring (1977) maintained the assumption of the radiative transparency of the emulsion, but decreased the thickness of the gas film between the immersed surface and the bed to $0.08\bar{d}_p$ from the value of $0.5\bar{d}_p$ assumed by both Vedamurthy and Sastri, and Bhattacharya and Harrison. In another variation of the model of Vedamurthy of Sastri, Zhang et al. (1984) assume the gas film thickness to be $0.154\bar{d}_p$, and the radiative transfer between plates to be more than one plate deep. A signif-

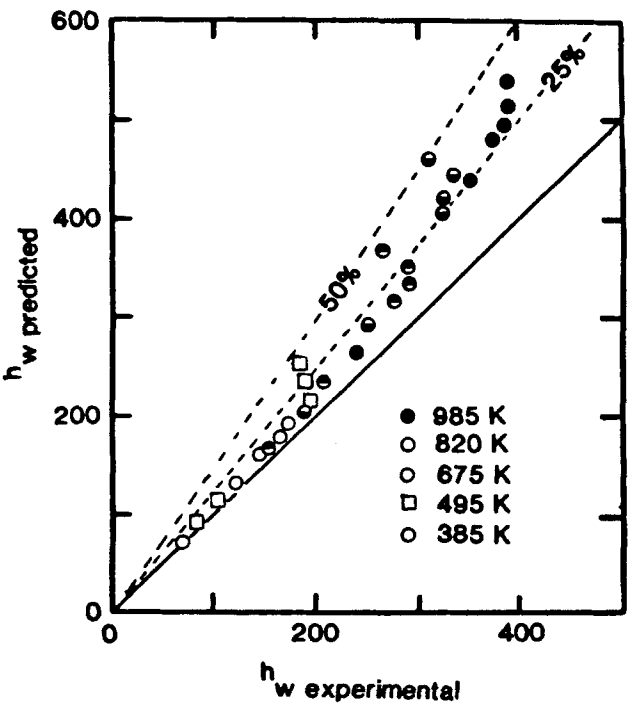

Figure 10. Comparison of experimental h_w values with predictions from model of Yoshida et al. (1974).
559 μm sand particle bed

icantly different approach has been adopted by Kolar et al. (1979), who model the emulsion as a series of alternate slabs of gas and solids. The heat transfer through the solid slabs is by conduction alone, while that across the gas slabs occurs by both conduction and radiation. Borodulya and Kovensky (1983) model the parallel plates as two-dimensional planes with particles arranged on them in a regular grid. The radiation incident on each plate is assumed to undergo reflection, radiation, and scattering, and the absorptivity, reflectivity, and transmissivity of an individual plate are calculated on the basis of the geometric configuration of the particles. The limiting values of these parameters as the number of plates in the stack approaches infinity are considered to be the effective bed values.

The prediction of h_w at high temperatures from the models of Yoshida et al. (1974) and Glicksman and Decker (1985) is next compared with the experimental data obtained in this study. The total heat transfer coefficient h_w predicted by the model of Yoshida et al. is given by the following expression:

$$h_w = (1 - \delta_B)(k_e \rho_e C_{ps}/\tau)^{1/2} + \delta_B \sigma \epsilon_t (T_b^2 + T_t^2)(T_b + T_t). \quad (39)$$

The effective packet density is assumed to be:

$$\rho_e = \rho_s(1 - \epsilon_{mf}). \quad (40)$$

The packet residence time and the bubble fraction were calculated from the correlations due to Thring (1977), and the effective thermal conductivity was calculated from the model of Kunii and Smith (1960).

Figures 11 and 12 show the comparison of the h_w values predicted by Eq. 39 with the experimentally obtained values for the two particles. The predicted values are greater than the experimental values except at very low fluidizing velocities. The overprediction is greater for the 559 μm sand beds than for the 751 μm beds when compared at the same temperature of 675 K. This trend clearly points out that the lack of a gas film resistance in the model of Yoshida et al. (1974) causes it to predict h_w values higher than those obtained experimentally. In this particle size range, and probably for all particle beds belonging to groups I and IIA, it is estimated that the model of Yoshida et al. overpredicts the experimental data by about 50%.

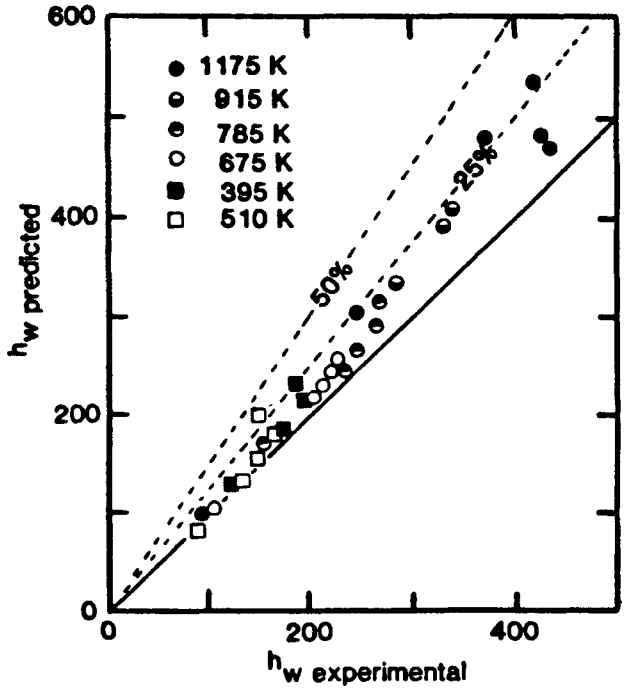

Figure 11. Comparison of experimental h_w values with predictions from model of Yoshida et al. (1974).
751 μm sand particle bed

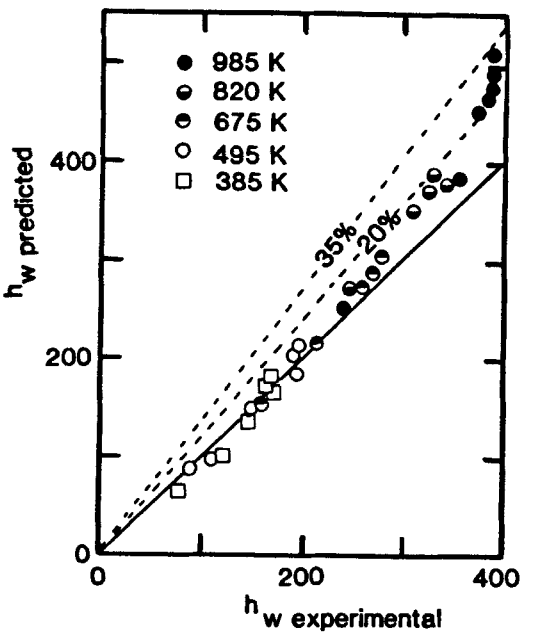

Figure 12. Comparison of experimental h_w values with predictions from model of Glicksman and Decker (1985).
559 μm sand particle bed

Figures 12 and 13 show similar comparison of the experimental h_w values with those predicted by the model of Glicksman and Decker (1985). The emulsion phase flux, q_e, is obtained from the following:

$$q_e = \frac{(T_b - T_t)}{R_w + R_e} \quad (41)$$

where

$$\frac{1}{R_w} = \frac{6k_g}{\bar{d}_p} + \frac{\sigma(T_t^2 - T_t^2)(T_t + T_t)}{(1/\epsilon_t) + (1/\epsilon_b) - 1} \quad (42)$$

and

$$\frac{1}{R_e} = (4k_e \rho_e C_{ps}/\pi\tau)^{1/2}. \quad (43)$$

ρ_e, τ, and f_B are calculated as described earlier, and k_e is calculated from:

$$k_e = k_{eo} + k_r \quad (44)$$

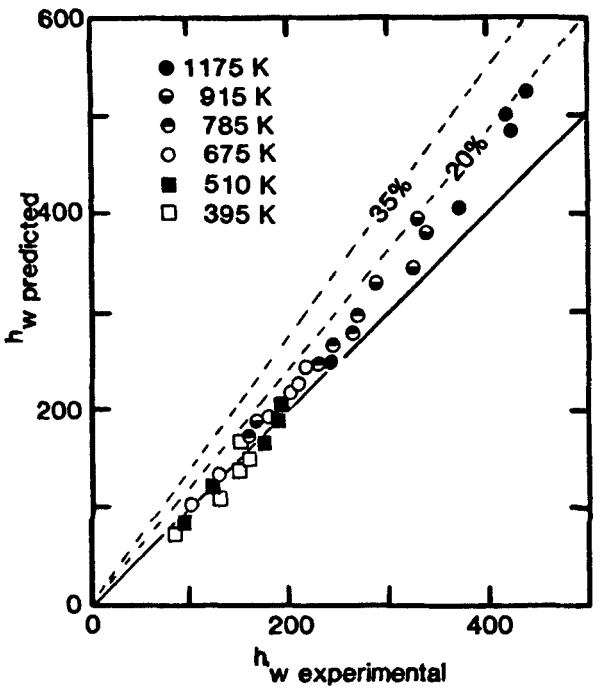

Figure 13. Comparison of experimental h_w values with predictions from model of Glicksman and Decker (1985).

751 μm sand particle bed

where k_{eo} is the thermal conductivity at ambient temperature from the model of Kunii and Smith (1960). k_r has been calculated, following the recommendation of Glicksman and Decker (1985), by the following expression due to Hill and Wilhelm (1959):

$$k_r = (4/9)\bar{d}_p \sigma T_b^3. \tag{45}$$

q_B is also calculated from Eq. 41, but with R_w set equal to zero. Equation 5 is then used to determine q. Finally, h_w is computed using the relationship of Eq. 11.

The predictions from this model are in good agreement with the experimental data, most being within ±20%. The model overpredicts the h_w values at high temperatures, and this overprediction increases with increase in temperature. This is probably due to the plane-parallel approximation of the tube-interface geometry. Also, the reliability of Eq. 42 has not been established, and the use of other correlations for k_e at high temperatures could result in better predictions. It should be noted, however, that the maximum overprediction by this model is less than 35%, which is remarkable considering its simplicity. It is therefore recommended that this model be used for estimating h_w at high temperatures.

Acknowledgment

The authors would like to record their gratitude to J. C. Chen and J. R. Welty, from whose recent works in this area they have learned and derived much inspiration. Partial support of this work from the National Science Foundation is also acknowledged.

Notation

b = constant, Eq. 33
C_1–C_4 = constants
d = equivalent thickness of quartz glass window and emulsion phase thermal boundary layer, m
$\bar{d}_p$ = average particle diameter, m
f_B = time fraction for which a probe is exposed to bubbles
h_w = overall heat transfer coefficient between bed and an immersed surface, W/m² · K
h_{wB} = heat transfer coefficient between a bubble and an immersed surface, W/m² · K
h_{wc} = convective heat transfer coefficient between bed and an immersed surface, W/m² · K
h_{we} = heat transfer coefficient between emulsion phase and an immersed surface, W/m² · K
h_{wgc} = component of h_w due to gas convection, W/m² · K
h_{wpc} = component of h_w due to particle convection, W/m² · K
h_{wmax} = maximum value of h_w, W/m²
h_{wr} = radiative heat transfer coefficient between bed and an immersed surface, W/m² · K
k_e = effective bed thermal conductivity, W/m · K
k_{eo} = effective bed thermal conductivity at ambient temperature, W/m · K
k_g = thermal conductivity of fluidizing gas, W/m · K
k_p = thermal conductivity of probe material, W/m · K
k_q = thermal conductivity of quartz glass, W/m · K
k_r = component of k_e due to radiation, W/m · K
q = heat flux at probe surface, W/m²
q_B = bubble phase heat flux at probe surface, W/m²
q_C = heat flux measured by fluxmeter C of high-temperature heat transfer probe, W/m²
q_{gc} = gas convective heat flux at probe surface, W/m²
q_{gcB} = bubble phase gas convective flux at probe, W/m²
q_{gce} = emulsion phase gas convective flux at probe, W/m²
q_1 = conductive flux at fluxmeter C in high-temperature heat transfer probe, W/m²
q_{1o} = convective flux at quartz glass window, W/m²
q_{pc} = particle convective flux at probe surface, W/m²
q_{pce} = emulsion phase particle convective flux at probe, W/m²
q_r = radiative heat flux at probe surface, W/m²
q_{rB} = bubble phase radiative flux at probe, W/m²
q_{re} = emulsion phase radiative flux at probe, W/m²
R_e = emulsion phase heat transfer resistance, m² · K/W
R_w = heat transfer resistance of gas film at probe wall, m² · K/W
t_q = transmissivity of quartz glass
T_b = bed temperature, K
T_{Bi} = temperature of inner face of fluxmeter B, K
T_{Bo} = temperature of outer face of fluxmeter B, K
T_{Ci} = temperature of inner face of fluxmeter C, K
T_{Co} = temperature of outer face of fluxmeter C, K
T_I = temperature of particles adjacent to heat transfer surface, K
T_q = temperature in quartz glass window, K
$\bar{T}_q$ = average temperature of quartz glass window, K
T_{qi} = temperature of inner face of quartz glass window of high-temperature heat transfer probe, K
T_{qo} = temperature of outer face of quartz glass window in high-temperature heat transfer probe, K
T_t = surface temperature of heat transfer probe, K
U_{mf} = superficial gas velocity at minimum fluidization, m/s
x = length coordinate, m
x_B = thickness of fluxmeter B, m
x_C = thickness of fluxmeter C, m
x_g = thickness of air gap in radiative fluxmeter, m
x_q = thickness of quartz glass window, m

Greek letters

α = absorptivity of quartz glass window
δ_B = bubble fraction in bed
ϵ = bed voidage
ϵ_{mf} = bed voidage at minimum fluidization
ϵ_t = emissivity of heat transfer probe surface
ρ_e = emulsion phase density, kg/m³
ρ_s = solids density, kg/m³
σ = Stefan-Boltzmann constant, W/m² · K⁴
τ = particle residence time at heat transfer surface, s

Literature cited

Alavizadeh, N., R. L. Adams, J. R. Welty, and A. Goshayeshi, "An Instrument for Local Radiative Heat Transfer Measurement in a Gas-Fluidized Bed at Elevated Temperatures," *22nd AIChE/ASME Nat. Heat Transfer Conf.*, Niagara Falls (1984).

Alavizadeh, N., Z. Fu, R. L. Adams, J. R. Welty, and A. Goshayeshi, "Radiative Heat Transfer Measurements for a Horizontal Tube Immersed in Small and Large Particle Fluidized Beds," *Int. Symp. Heat Transfer*, Beijing (1985).

Baskakov, A. P., B. V. Berg, O. K. Vitt, N. F. Fillipovsky, V. A. Kirakosyan, J. M. Goldobin, and V. K. Maskaev, "Heat Transfer to Objects Immersed in Fluidized Beds," *Powder Technol.*, **8**, 273 (1973).

Basu, P., "Bed-to-Wall Heat Transfer in a Fluidized Bed Coal Combustor," *AIChE Symp. Ser. No. 176*, **74**, 187 (1978).

Bhattacharya, S. C., and D. Harrison, "Heat Transfer in High-Temperature Fluidized Beds," *Eur. Congr. Particle Technol.* Nuremberg, p. 23, Session K2 (1977).

Borodulya, V. A., and V. I. Kovensky, "Radiative Heat Transfer between a Fluidized Bed and a Surface," *Int. J. Heat Mass Transfer*, **26**(2), 277 (1983).

Botterill, J.S.M., Y. Teoman, and K. R. Yuregir, "Factors Affecting Heat Transfer between Gas-Fluidized Beds and Immersed Surfaces," *Powder Technol.*, **39**, 177 (1984).

Chen, J. C., and K. L. Chen, "Analysis of Simultaneous Radiative and Conductive Heat Transfer in Fluidized Beds," *Chem. Eng. Commun.*, **9**, 225 (1981).

Flamant, G., "Theoretical and Experimental Study of Radiant Heat Transfer in a Solar Fluidized-Bed Receiver," *AIChE J*, **28**, 529 (1982).

Ganzha, V. L., S. N. Upadhyay, and S. C. Saxena, "A Mechanistic Theory for Heat Transfer between Fluidized Beds of Large Particles and Immersed Surfaces," *Int. J. Heat Mass Transfer*, **25**(10), 1531 (1982).

Gelperin, N. I., and V. G. Einshtein, "Heat Transfer in Fluidized Beds," *Fluidization*, J. F. Davidson and D. Harrison, eds., Academic Press, New York, 471 (1971).

George, A. H., and J. R. Welty, "Local Heat Transfer Coefficients for a Horizontal Tube in a Large-Particle Fluidized Bed at Elevated Temperatures," *AIChE J*, **30**, 482 (1984).

Glicksman, L., and N. A. Decker, "Heat Transfer from an Immersed Surface to Adjacent Particles in a Fluidized Bed: The Role of Radiation and Particle Packing," *Proc. 8th Int. Conf. Fluidized-Bed Combust.*, Houston, 45 (1985).

Goshayeshi, A., J. R. Welty, R. L. Adams, and N. Alavizadeh, "Local Heat Transfer Coefficients for Horizontal Tube Arrays in High-Temperature Large-Particle Fluidized Beds—An Experimental Study," *AIChE Symp. Ser. No. 245*, **81**, 34 (1985).

Grewal, N. S., and S. C. Saxena, "Heat Transfer between a Horizontal Tube and a Gas-Solid Fluidized Bed," *Int. J. Heat Mass Transfer*, **23**, 1505 (1980).

Hill, F. B., and R. H. Wilhelm, "Radiative and Conductive Heat Transfer in a Quiescent Gas-Solid Bed of Particles: Theory and Experiment," *AIChE J.* **5**, 486 (1959).

Il'chenko, A. I., V. S. Pishakov, and K. E. Makhorin, "Study of Radiative Heat Transfer in a Fluidized Bed," *J. Eng. Physics*, **14**(4), 321 (1968).

Jolley, L. J., "Heat Transfer in Beds of Fluidized Solids," *Fuel*, **28**(5), 114 (1949).

Kellet, B. S., "The Steady Flow of Heat Through Hot Gases," J. Opt. Soc. America, **42**(5) 339 (1952).

Kolar, A. K., N. S. Grewal, and S. C. Saxena, "Investigation of Radiative Contribution in a High-Temperature Fluidized Bed Using the Alternate Slab Model," *Int. J. Heat Mass Transfer*, **22**, 1695 (1979).

Kunii, D., and J. M. Smith, "Heat Transfer in Porous Rocks," *AIChE J.*, **6**, 71 (1960).

Mickley, H. S., and D. F. Fairbanks, "Mechanism of Heat Transfer to Fluidized Beds," *AIChE J.*, **1**(3), 374 (1955).

Ozkaynak, T. F., J. C. Chen, and T. R. Frankenfield, "An Experimental Investigation of Radiation Heat Transfer in a High-Temperature Fluidized Bed," *Fluidization*, D. Kunii and R. Toei, eds., *Eng.* Foundation, New York (1984).

Panov, O. M., A. P. Baskakov, Yu. M. Goldobin, N. F. Fillipovskii, and Yu. S. Mazur, "Experimental Investigation of the Radiant and Conductive-Convective Components of External Heat Exchange in a High-Temperature Fluidized Bed," *J. Eng. Phys.*, **36**, 275 (1979).

Saxena, S. C., and V. L. Ganzha, "Heat Transfer to Immersed Surfaces in Gas-Fluidized Beds of Large Particles and Powder Characterization," *Powder Technol.*, **39**, 199 (1984).

Saxena, S. C., and A. Mathur, "Hydrodynamic and Heat Transfer Studies in Fine-Particle Gas-Solid Fluidized Beds," *Energy*, **10**, 57 (1985).

Szekely, J., and R. J. Fisher, "Bed-to-Wall Radiation Heat Transfer in a Gas-Solid Fluidized Bed," *Chem. Eng. Sci.*, **24**, 833 (1969).

Thring, R. H., "Fluidized Bed Combustion for the Stirling Engine," *Int. J. Heat Mass Transfer*, **20**, 911 (1977).

Touloukian, Y. S., R. W. Powell, C. Y. Ho, and P. G. Klemens, *Thermophysical Properties of Matter*, Vol. 1. *Thermal Conductivity: Metallic Elements and Alloys*, IFI/Plenum, New York (1970).

Tuzla, K., S. Biyikli, J. C. Chen, "Experimental Measurement of Heat Transfer in High-Temperature Fluidized Beds," *Proc. 8th Int. Conf. Fluidized-Bed Combust.*, 159 (1958).

Vadivel, R., and V. N. Vedamurthy, "An Investigation of the Influence of Bed Parameters on the Variation of the Local Radiative and Total Heat Transfer Coefficient Around an Embedded Horizontal Tube in a Fluidized Bed Combustor," *Proc. 6th Int. Conf. Fluidized-Bed Combust.*, 111, 1159 (1980).

Vedamurthy, V. N., and V. M. K. Sastri, "An Analysis of the Conductive and Radiative Heat Transfer to the Walls of Fluidized-Bed Combustors," *Int. J. Heat Mass Transfer*, **17**, 1 (1974).

White, T. R., A. Mathur, and S. C. Saxena, "Effect of Vertical Boiler Tube Diameter on Heat Transfer Coefficient in Gas-Fluidized Beds," *Chem. Eng. J.*, **32**, 1 (1986).

Wright, S. J., R. Hickman, and H. C. Ketley, "Heat Transfer in Fluidized Beds of Wide Size Spectrum at Elevated Temperatures," *Brit. Chem. Eng.*, **15**, 1551 (1970).

Yoshida, K., T. Ueno, and D. Kunii, "Mechanisms of Bed-Wall Heat Transfer in a Fluidized Bed at High Temperatures," *Chem. Eng. Sci.*, **29**, 77 (1974).

Zhang, H., and C. Xie, "The Radiative Heat Transfer of the Immersed Tube in a Fluidized-Bed Combustor," *Proc. 8th Int. Conf. Fluidized-Bed* Combust. Houston, 142 (1985).

Zhang, H., K. Cen, and G. Huang, "Heat Transfer to the Immersed Tubes in Fluidized-Bed Combustion of Low-Grade Coal," *Int. Chem. Eng.*, **24**(1), 158 (1984).

Manuscript received July 3, 1986, and revision received Dec. 9, 1986.